# Material tests report

## Wrapped Composite Joints project

by **Vasilis Mylonopoulos**

| | |
|---|---|
| Course: | **CIE5050-09** - Additional Graduation Work |
| Instructors: | Dr. M. Pavlovic, Pei He (PhD cand.) |
| Institution: | Delft University of Technology |
| Place: | Faculty of Civil Engineering and Geosciences, Delft |
| Project Duration: | November, 2020 - February, 2021 |

# Contents

**1 Introduction** **1**

**2 Coupon Testing Summary** **2**
2.1 Results . . . 2
2.2 Test Standards-Procedure . . . 2

**3 Material-Coupon Info** **2**
3.1 Coupons Geometry . . . 2

**4 Experiments** **5**
4.1 In Plane Shear (IPS) tests . . . 5
4.1.1 Coupons dimensions . . . 5
4.1.2 Results . . . 5
4.2 Tensile (T) tests . . . 10
4.2.1 Coupons dimensions . . . 10
4.2.2 Results . . . 10
4.3 Compression (C) tests . . . 15
4.3.1 Coupons dimensions . . . 15
4.3.2 Results . . . 15
4.4 Compact Tension (CT) tests . . . 21
4.4.1 Specimens dimensions . . . 21
4.4.2 Results . . . 22

**5 Concluding remarks** **31**

**References** **32**

# 1 Introduction

Interest in composites for application in Civil Engineering structures, has seen significant increase in recent years. From composite repairs on existing structures from concrete or structural steel, to composite decks in bridges or even structures made solely out of fibre reinforced composites, the structural industry is following the already existing trend in automotive and aerospace industry where composite solutions present a great potential that traces back to 1960's. Within this framework the Wrapped Composite Joints project, under Dr. M. Pavlovic, attempts to bring the composites technology to jacket designs of offshore wind turbines and replace the traditional welding technology that is used for connecting the steel tubular members of the jacket frame. Higher stiffness, more sustainable and lightweight design due to reduced steel weight and most importantly higher fatigue resistance are just some of the benefits that the developing technology brings in the structure.

Developing a new technology especially when a novel material solution is used, requires robust knowledge of the inherent material as well as bond properties. For this experimental testing series should take place along different structural levels. Goal of such experimental series is to investigate the capabilities of the material as well as the assembled components up to total failure.

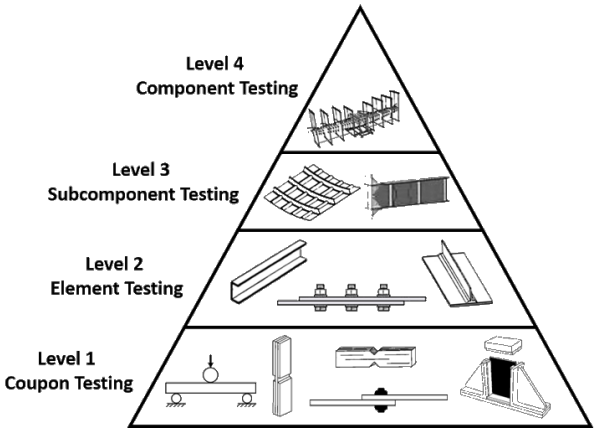


Figure 1: Building block approach for composite structures (https://www.compositesworld.com).

In the current Additional graduation work a coupon testing series comprising of different standard test methods, part of the Wrapped Composite joints project is presented. Aim of this study is the establishment of fundamental material elastic as well as fracture properties for the composite layup used in the project. Outcomes of the experimental study will be used as input for the realistic representation of the material and the bonded interface through Finite Element Models(FEM) of several scales, from small specimens to large and full scale Joints.

# 2 Coupon Testing Summary

## 2.1 Results

As part of the Wrapped Composites Joint demonstrator project, a series of coupon tests were conducted in Stevin II Lab, in order to determine the mechanical properties of the woven mat used. This series included **In Plane Shear (IPS)**, **Tensile (T)**, **Compression (C)** and **Compact Tension (CT)** experiments. Specimens were loaded to failure. Below an average value of the results, together with the 95% confidence interval of the data are given:

| **Elastic properties** | |
|---|---|
| Elastic modulus in fibre direction* | $E_1 = 11937.6 \pm 601$ MPa |
| Shear Modulus | $G_{12} = 3.12 \pm 0.9$GPa |
| Tensile strength in fibre direction | $\sigma_{1max} = 216.18 \pm 10.96$ MPa |
| In plane shear strength | $\tau_{12max} = 72.19 \pm 1.64$ MPa |
| Tensile strain to failure in fibre direction | $\epsilon_{1f} = 2.33 \pm 0.21\%$ |
| Shear strain to failure | $\gamma_{12f} = 4.6 \pm 0.27\%$ |
| Poisson's ratio | $\nu_{12} = 0.15 \pm 0.0083$ |
| **Fracture properties** | |
| Mode I translaminar fracture toughness | $G_{IC} = 63.44 \pm 9.4$ N/mm |

Table 1: Experimental results summary

*Elastic modulus value corresponds to the average value of the values obtained from the tensile and compression experiments.

## 2.2 Test Standards-Procedure

For the determination of the abovementioned properties different ISO standards were used. **ISO 14129**[1] was used for shear properties determination, **ISO 527-1,4** [2] for the tensile properties, **ISO 14126**[3] for the compressive properties and **ISO 13586**[4] and ASTME399 [5] for the intralaminar fracture toughness determination through CT testing. 9 coupons for T, IPS, and C experiments were tested, while for the CT 5 specimens were tested in quasi static loading.The **Instron 1251** machine in the TU Delft Stevin II Lab with a **100 kN** cell for static and a **200kN** cell for dynamic load was used to load the specimens in different speeds determined in the standards. Both 2D and 3D(Aramis) DIC system, together with data from the machine related software were used to record the force and strains during the tests. Commercial software GOM correlate was used for post process of the obtained DIC results.

# 3 Material-Coupon Info

## 3.1 Coupons Geometry

Geometry of the coupons, that were used for each type of experimental testing, is presented in the following pictures:

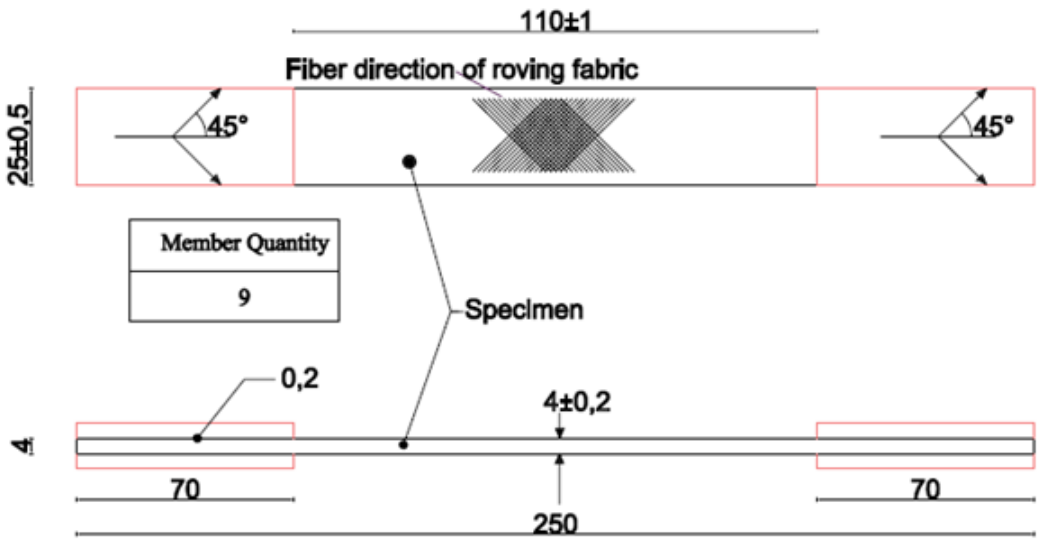


Figure 2: Geometry of IPS testing specimen.

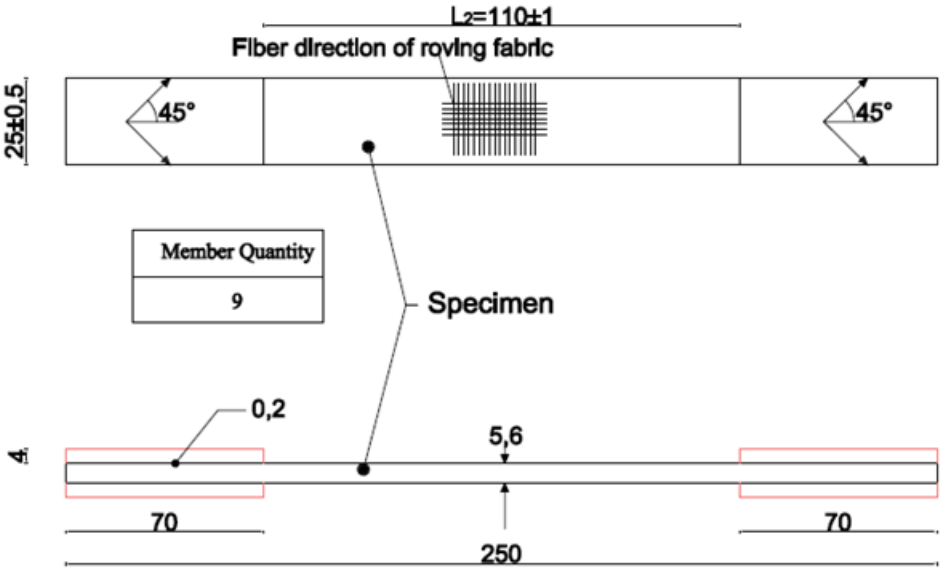


Figure 3: Geometry of Tensile testing specimen.

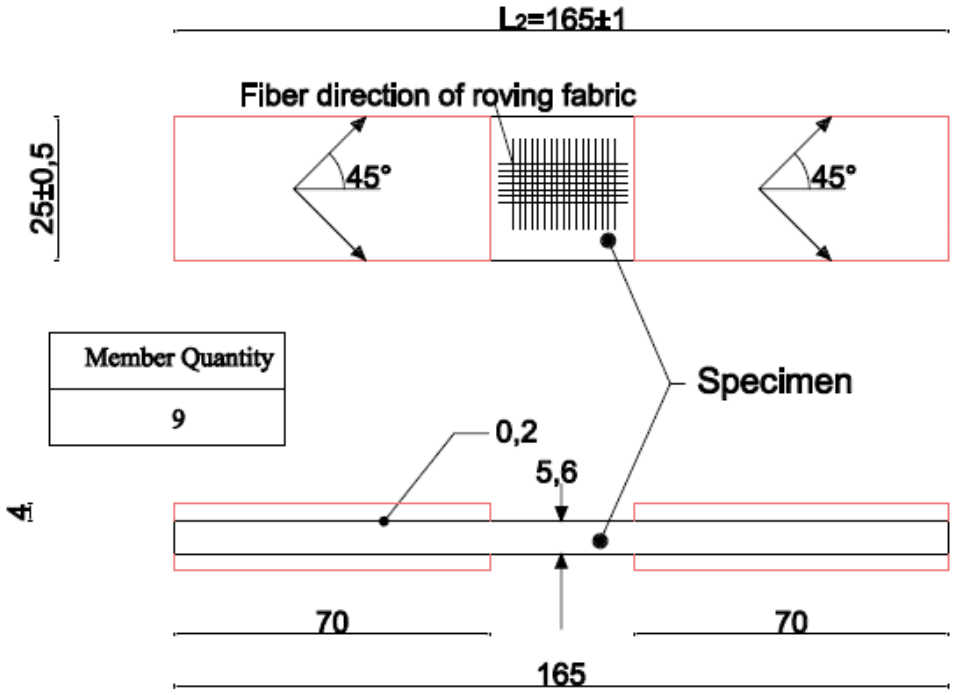


Figure 4: Geometry of Compression testing specimens

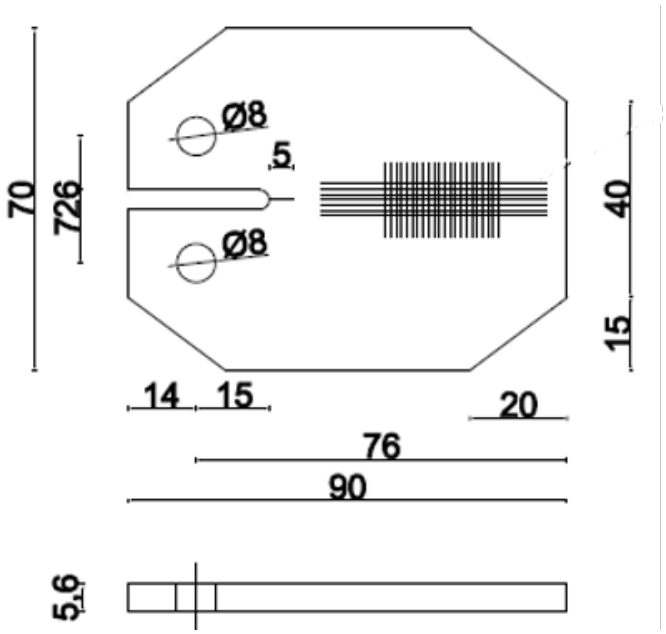


Figure 5: Geometry of Compact Tension specimens.

# 4 Experiments

## 4.1 In Plane Shear (IPS) tests

### 4.1.1 Coupons dimensions

For the In-Plane Shear coupons the prefix **TX** is used.

| **Coupon ID** | **TX02** | **TX03** | **TX04** | **TX05** | **TX06** | **TX07** | **TX08** | **TX09** |
|---|---|---|---|---|---|---|---|---|
| $b_m$(mm) | 28.67 | 26.07 | 28.5 | 28.93 | 28.76 | 28.8 | 28.63 | 27 |
| $b_r$(mm) | 28.66 | 26.26 | 28.42 | 28.82 | 28.54 | 28.78 | 28.72 | 27.05 |
| $b_l$(mm) | 28.41 | 26.66 | 28.58 | 29 | 28.87 | 28.93 | 28.40 | 26.95 |
| $h_m$(mm) | 4.91 | 4.36 | 4.37 | 4.78 | 4.62 | 4.43 | 4.28 | 4.58 |
| $h_r$(mm) | 4.93 | 4.08 | 4.42 | 4.83 | 4.65 | 4.89 | 4.27 | 4.66 |
| $h_l$(mm) | 4.48 | 4.24 | 4.24 | 4.62 | 4.37 | 4.37 | 4.73 | 4.42 |
| $b_{avg}$(mm) | 28.58 | 26.33 | 28.50 | 28.92 | 28.72 | 28.84 | 28.58 | 27 |
| $h_{avg}$(mm) | 4.77 | 4.23 | 4.34 | 4.74 | 4.55 | 4.56 | 4.43 | 4.55 |
| A($mm^2$) | 136.42 | 111.29 | 123.78 | 137.16 | 130.59 | 131.59 | 126.53 | 122.94 |

Table 2: IPS coupons dimensions.

### 4.1.2 Results

For the extraction of the results, [1] was used. The coupons were loaded at a displacement rate of **0.3mm/s (2mm/min)**, force-displacement data was recorded every 1 second, while photos were taken at time intervals of 2 seconds. In order to avoid slip of the coupons at the clamps of the machine, the pressure of the clamps was each time set to approximately the pressure needed for a load four times the expected maximum load. This had to be set carefully, as the tabs used where made from the same material as the specimens, and therefore had a low crushing strength. According to **ISO 14129** results from test specimens that fail **at or inside the tabs area** used for clamping shall be discarded. Coupons **TX06, TX07, TX09** were not considered in the statistical analysis of the data because of rupture close or inside the tabs. Therefore, five specimens, which corresponds to the minimum number of specimens set in the standard were used for extraction of the mechanical properties.

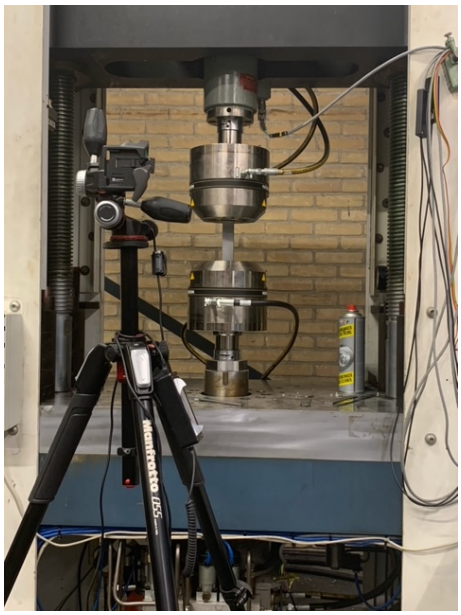


Figure 6: IPS test setup.

According to [1] the shear stress, during the experiment is calculated as:

$$\tau_{12} = \frac{F}{2 \cdot b \cdot h}$$

where **F** is the instantaneous load in newtons, while **b** and **h** represent the width and the height of the specimens respectively. For the maximum attained load during the loading history, the shear strength is calculated in the same manner where in the place of F the maximum load $F_m$ is used. The in-plane shear strain of the specimen is calculated as :

$$\gamma_{12} = \epsilon_x - \epsilon_y$$

where $\epsilon_x$ and $\epsilon y$ are the strains obtained using virtual extensometers in the middle of the specimens during the DIC analysis of the results. In figure 10 $\epsilon_x$ are shown in the positive half of the graph while $\epsilon y$ in the negative. According to ISO 14129 [1] strain gauges or extensometers used for the strain measurements shall be accurate to $\pm 1\%$ of the full scale. For the current study where the Field of View is equal to 150 x 100 mm, the accuracy of the DIC system would approximately be 150/50000 = 0.003 mm and therefore the requirement set by the standard applies.

(a) Photos before DIC analysis.

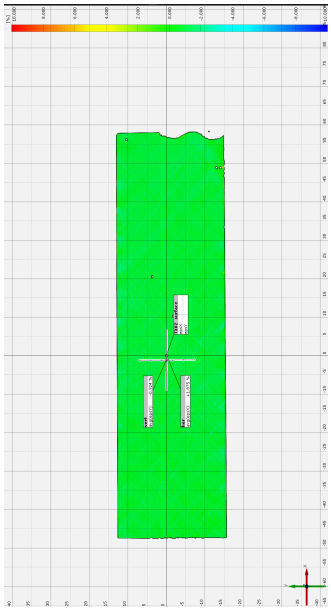

(b) Virtual extensometers during DIC analysis.

Figure 7: DIC analysis of IPS specimens.

The shear modulus $G_{12}$ is calculated as the slope of the stress-strain curve within the range of 0.001 and 0.005 shear strain.

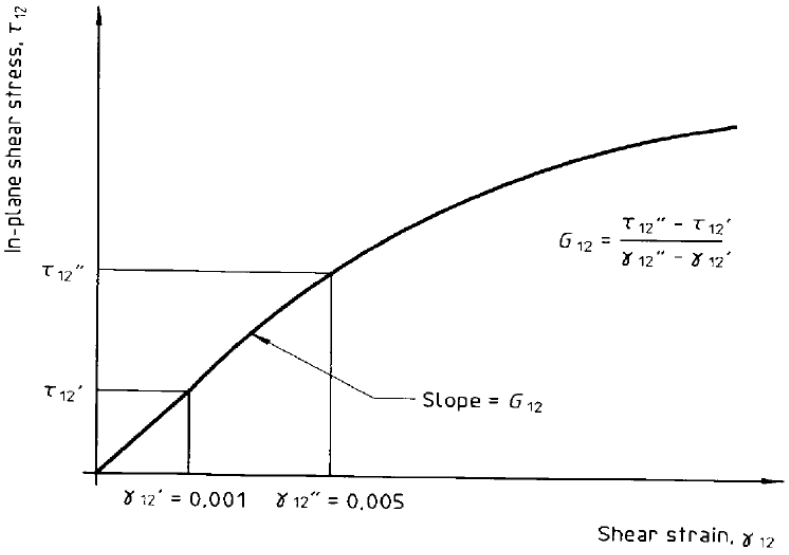


Figure 8: Typical shear stress-strain graph as presented in [1].

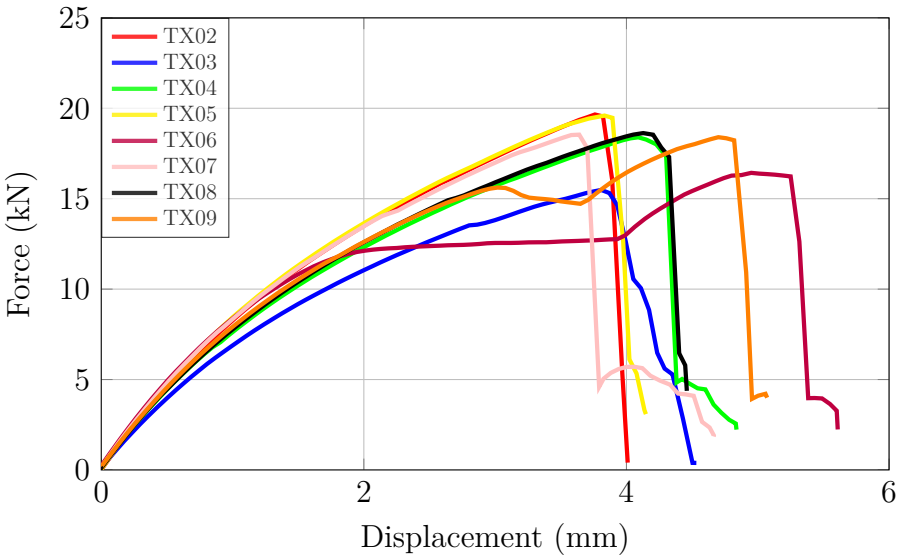


Figure 9: IPS Force-Displacement graph.

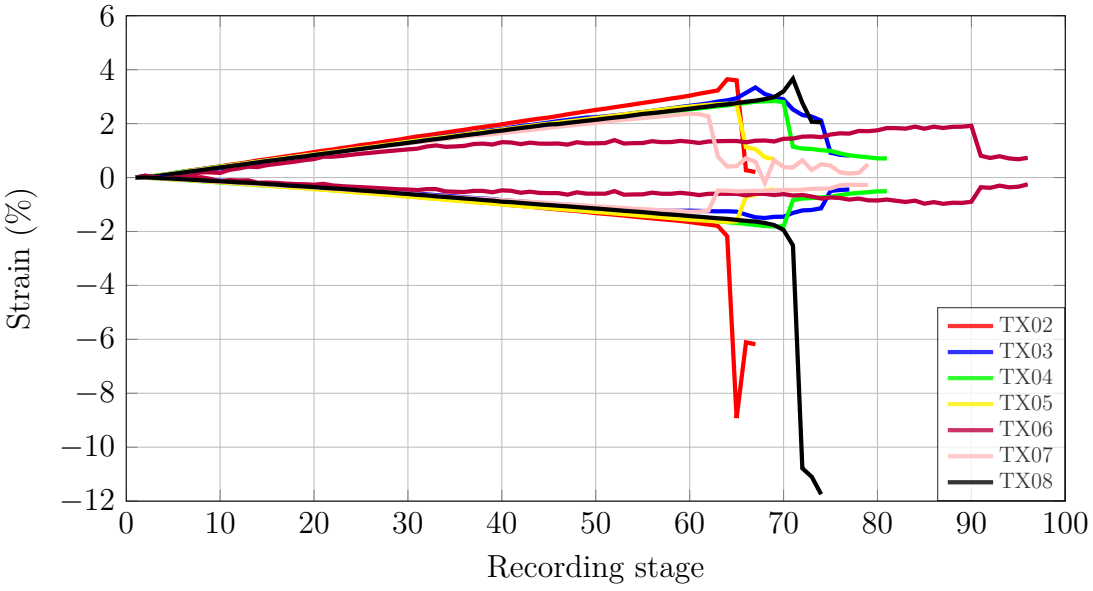


Figure 10: IPS Longitudinal strains vs recording stage.

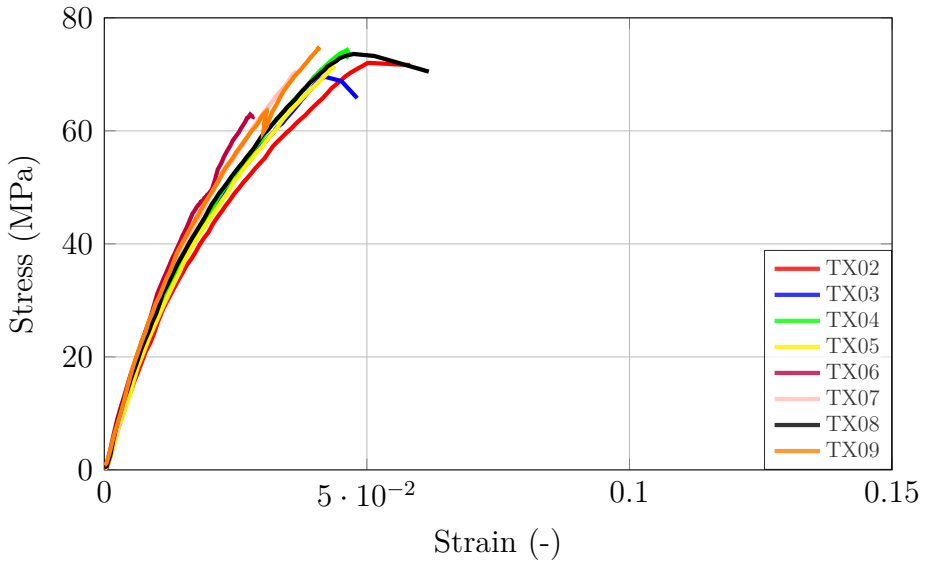


Figure 11: IPS Stress-Strain graph.

| **Coupon** | **Shear Modulus(GPa)** | **Shear strength(MPa)** | **Strain at failure(-)** |
|---|---|---|---|
| TX02 | 2.94 | 72.04 | 0.050 |
| TX03 | 3.04 | 69.56 | 0.042 |
| TX04 | 3.22 | 74.30 | 0.046 |
| TX05 | 2.96 | 71.43 | 0.044 |
| TX06 | - | - | - |
| TX07 | - | - | - |
| TX08 | 3.45 | 73.60 | 0.047 |
| TX09 | - | - | - |
| **Mean** | **3.12** | **72.19** | **0.046** |
| **95% confidence interval** | 0.19 | 1.64 | 0.003 |
| **Standard Deviation** | 0.21 | 1.87 | 0.003 |
| **COV(%)** | 6.81 | 2.58 | 6.90 |

Table 3: Results of In-Plane Shear testing.

Shear strength results, are considered the most reliable due to the low coefficient of variation (2.58 %), obtaining a shear strength of 72.19 MPa. A larger scatter is realised in the results of the strain to failure as well as the shear modulus, however not to a level that the results can not be considered reliable. The failure mode, in all coupons is satisfying, as the $\pm 45$ degree fibres are clearly overstretched and in the end fail. In general, the results show good correlation and can therefore be used for modelling purposes.

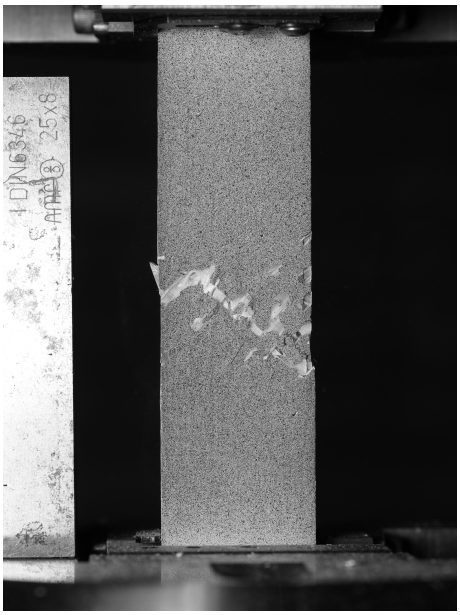

(a) IPS specimen right after failure.

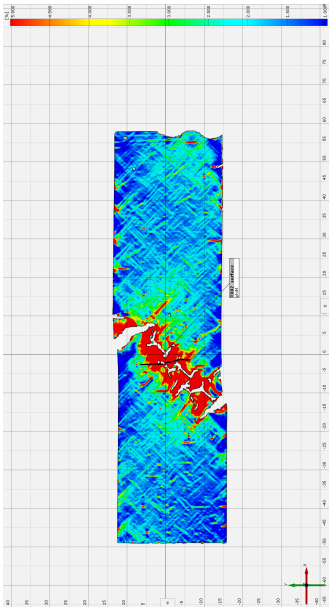

(b) Shear strains of IPS specimen at failure.

Figure 12: ± 45 degree failure pattern of IPS specimen (TX02).

## 4.2 Tensile (T) tests

### 4.2.1 Coupons dimensions

For the Tensile coupons the prefix **TM** is used.

| Coupon ID | TM01 | TM02 | TM03 | TM04 | TM05 | TM06 | TM07 | TM08 | TM09 |
|---|---|---|---|---|---|---|---|---|---|
| $b_m$(mm) | 29 | 28.93 | 29 | 25.68 | 29.34 | 28.96 | 28.98 | 27.50 | 29.14 |
| $b_r$(mm) | 29 | 28.93 | 29 | 25.60 | 29.33 | 29.02 | 28.84 | 27.40 | 29.15 |
| $b_l$(mm) | 29.05 | 28.87 | 28.99 | 25.90 | 29.28 | 28.96 | 29.05 | 27.61 | 29.19 |
| $h_m$(mm) | 7.96 | 7.49 | 7.60 | 7.63 | 7.48 | 7.48 | 7.48 | 7.43 | 7.58 |
| $h_r$(mm) | 7.80 | 7.70 | 7.64 | 7.65 | 7.60 | 7.25 | 7.48 | 7.35 | 7.34 |
| $h_l$(mm) | 7.30 | 7.58 | 7.32 | 7.25 | 7.51 | 7.55 | 7.45 | 7.72 | 7.51 |
| $b_{avg}$(mm) | 29.02 | 28.91 | 28.99 | 25.73 | 29.32 | 28.98 | 28.96 | 27.50 | 29.16 |
| $h_{avg}$(mm) | 7.69 | 7.59 | 7.52 | 7.51 | 7.53 | 7.43 | 7.47 | 7.50 | 7.48 |
| A($mm^2$) | 223.04 | 219.43 | 218.05 | 193.20 | 220.75 | 215.22 | 216.30 | 206.27 | 218.019 |

Table 4: T coupons dimensions.

### 4.2.2 Results

Tensile testing was conducted according to ISO 527-1,4 [2]. Coupons where put in the machine so that their major axis was aligned to the centre line of the grips assembly and were loaded at a displacement rate of **0.3mm/s** (2mm/min). Force-displacement data was recorded every 1 second while photos were taken every 2 seconds. For specimens TM01, TM02, TM03, TM06 2D DIC was used while for TM04, TM05, TM07, TM08, TM09 3D DIC was used instead. Out of a total of 9 specimens, only 5 of them namely

**TM02, TM05, TM06, TM08, TM09** were used for the statistical analysis, due to unacceptable failure modes. In the rest of the specimens **TM01, TM03, TM07, TM04** failure very close or inside the grip tab occurred which according to the standard meant that they should be discarded. The considerable number of specimens that failed in an undesirable way, can be explained by the poor quality of the grip tabs, where eccentricities existed. Those eccentricities can be responsible for certain local bending, or twist effects, while the clamps grabbed the specimens, resulting in failures quite close to the clamps. Visual observation of all the specimens, showed that the specimens with the less smooth and more eccentric tabs, are those that resulted to grip failures.

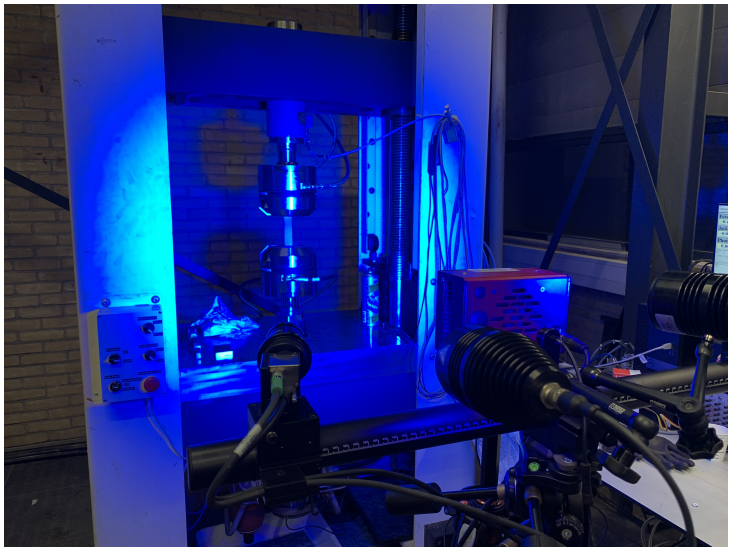

Figure 13: T testing setup with 3D DIC equipment.

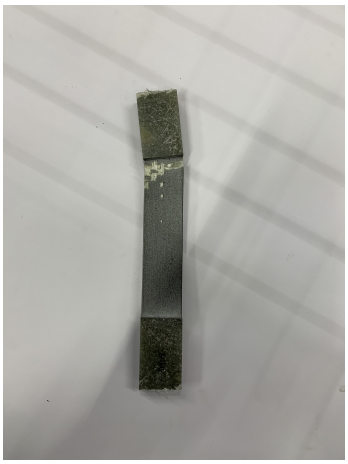

(a) T unacceptable failure mode.

(b) T acceptable failure mode.

Figure 14: T tests observed failure modes.

According to [2] the tensile strength is calculated as:

$$\sigma_{0max} = \frac{F_m}{A}$$

where $F_m$ is the maximum force in Newtons obtained during the loading history. The strain at failure, $\epsilon_m$ is taken as the strain at the point at which the tensile strength is

reached. The strains where determined using two virtual extensometers through the GOM correlate software, one 40mm in the longitudinal axis and one 20mm in the transverse direction, positioned at the middle of the specimen, the same way two physical extensometers would have been positioned. Again as in the case of In plane shear testing, ISO527 [2] specifies a requirement for the accuracy in the case of physical extensometers used fro strain measurements, being $\pm 1\%$ of the physical length. The area covered by the photos again produces accuracy of 150/50000=0.003mm and therefore the aforementioned requirement is satisfied.

$$\epsilon = \frac{\Delta L_0}{L_0}$$

The tensile elastic modulus ($E_t$) was determined by applying a least squares linear regression analysis on the stress strain curve on the strain interval $0.0005 \leq \epsilon \leq 0.0025$.

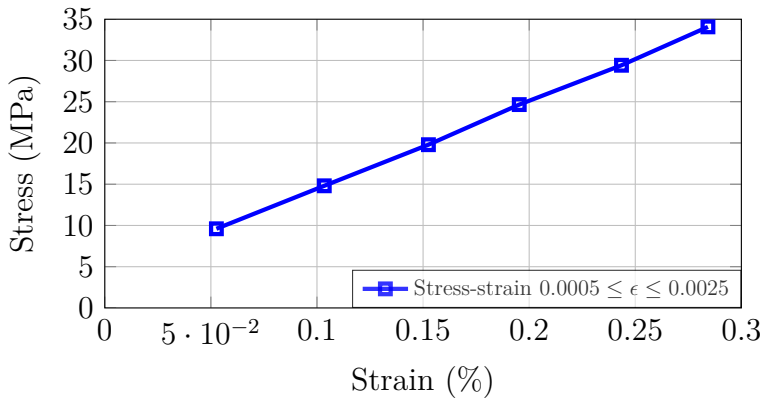


Figure 15: Elastic modulus calculation through virtual extensometers (TM01).

The Poisson's ratio was determined by plotting the change in length (strain in the X direction) against the change in width(strain in Y direction) of the specimen, according to the extensometer's measurements, and applying a least squares linear regression fit on the strain interval.

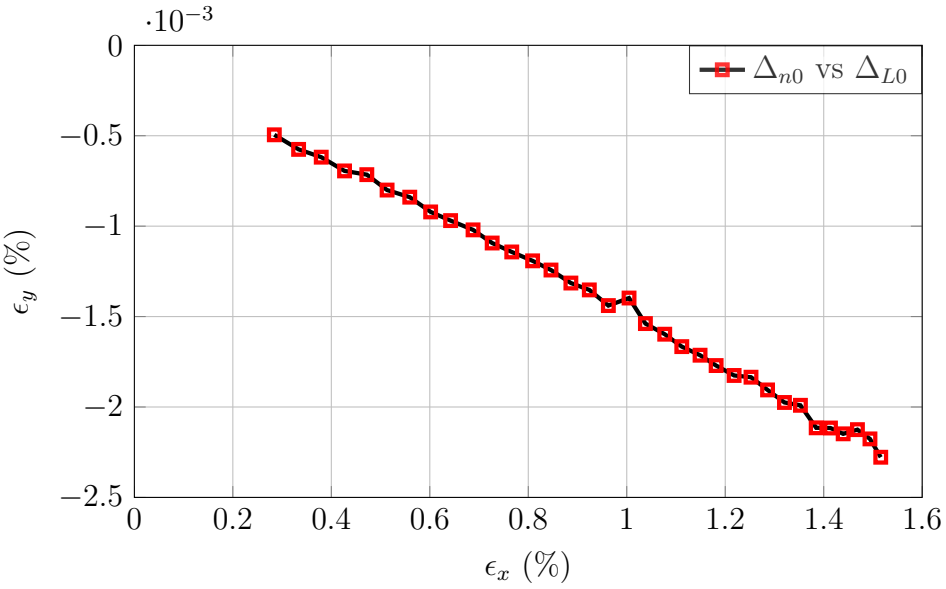


Figure 16: Poisson's ratio calculation example (TM01).

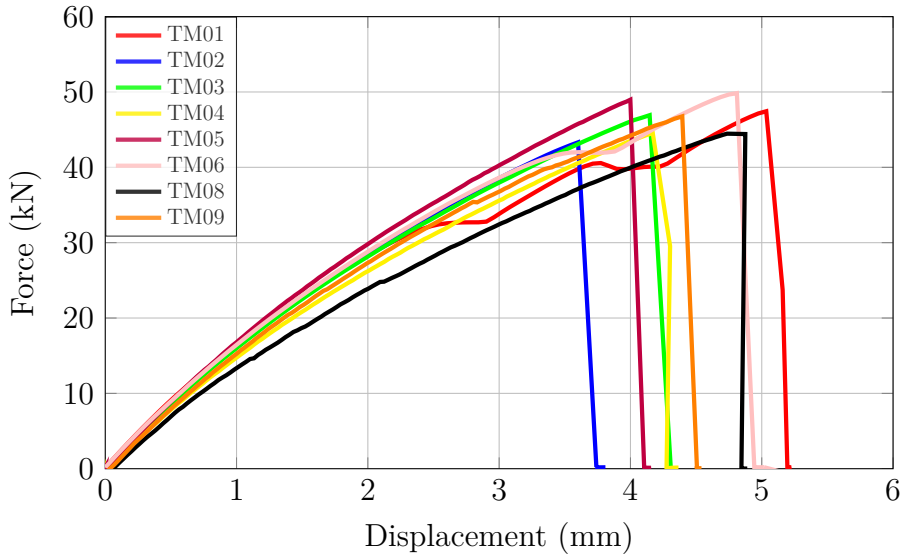


Figure 17: T Force-Displacement graph.

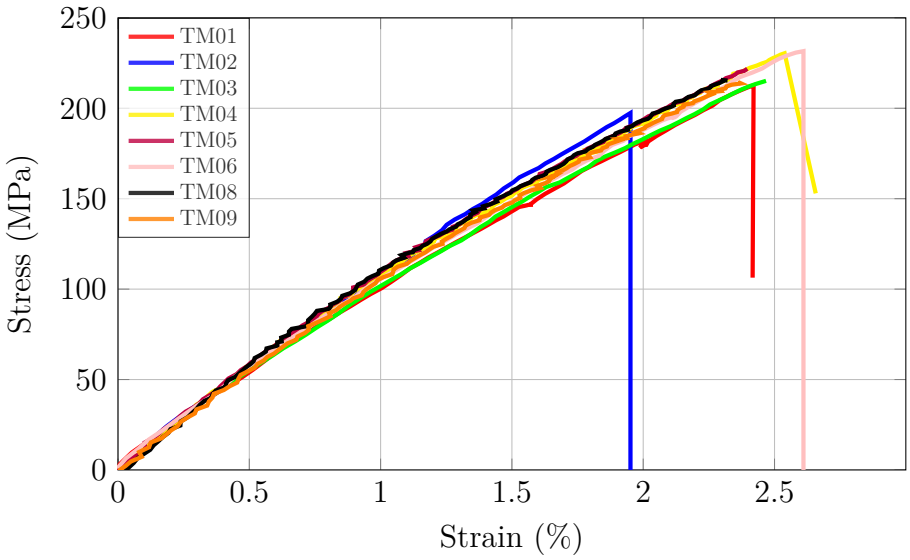


Figure 18: T Stress-Strain graph.

| **Coupon** | **Elastic Modulus (MPa)** | **Tensile strength (MPa)** | **Strain at failure(%)** | **Poisson's ratio ($v_{12}$)** | **Failure Mode** |
|---|---|---|---|---|---|
| TM01 | - | - | - | - | Grip failure |
| TM02 | 12050 | 197.39 | 1.95 | 0.15 | Close to tab |
| TM03 | - | - | - | - | Grip failure |
| TM04 | - | - | - | - | Grip failure |
| TM05 | 12562 | 221.84 | 2.39 | 0.15 | Away from the tab |
| TM06 | 10866 | 231.58 | 2.61 | 0.14 | Middle |
| TM07 | - | - | - | - | Grip failure |
| TM08 | 12365 | 215.57 | 2.32 | 0.13 | Close to tab |
| TM09 | 11148 | 214.49 | 2.36 | 0.15 | Away from the tab |
| **Mean** | **11798.2** | **216.17** | **2.33** | **0.1465** | |
| **95% confidence interval** | 658.82 | 10.96 | 0.21 | 0.008 | |
| **Standard Deviation** | 751.63 | 12.50 | 0.24 | 0.0095 | |
| **COV(%)** | 6.37 | 5.78 | 10.23 | 6.49 | |

Table 5: Results of Tensile testing.

As it can be observed by the stress strain curve presented two out of the five specimens used for the statistical analysis of the results, **TM02** and **TM06** appeared to have extreme values in terms of tensile strength. The remaining three specimens showed very good correlation in terms of strength, and the result of **216.18** MPa can be considered reliable enough due to the small coefficient of variation of the sample. In terms of stiffness,

more scatter can be detected, but still not up to a level, that can make the results unreliable. Comparing the presented results, with previous tensile experiments on the same material conducted by PhD candidate Pei He, reveals a good agreement, with smaller values obtained in this series of tests, explained by the number of discarded specimens as well as the failure modes of the used specimens. It should also be mentioned that in the two series different method of strain measurements was used. In Pei's experiments physical extensometers were used while in this study DIC.

| **Test series** | **Elastic Modulus (MPa)** | **Tensile strength (MPa)** | **Strain at failure(%)** |
|---|---|---|---|
| Pei He results | 12150 | 226.80 | 2.35 |
| Current study | 11798 | 216.18 | 2.33 |
| %difference | -2.28 | -4.70 | -0.85 |

Table 6: Comparison of Tensile test series.

## 4.3 Compression (C) tests

### 4.3.1 Coupons dimensions

For the Compression coupons the prefix **TK** is used.

| **Coupon ID** | **TK01** | **TK02** | **TK03** | **TK04** | **TK05** | **TK06** | **TK07** | **TK08** | **TK09** |
|---|---|---|---|---|---|---|---|---|---|
| b(mm) | 26.8 | 26.4 | 28.7 | 29.1 | 28.7 | 29.1 | 28.6 | 29 | 29.1 |
| h(mm) | 6.82 | 7.38 | 7.32 | 7.38 | 6.78 | 7.24 | 7.28 | 6.98 | 7.36 |
| A($mm^2$) | 182.77 | 194.83 | 210.08 | 214.76 | 194.58 | 210.68 | 208.21 | 202.42 | 214.17 |

Table 7: C coupons dimensions.

Compression specimens were designed and tested according to [3], ISO standard for determination of the in plane compressive properties of Fibre Reinforced Polymers. In this standard three types of specimens, as well as two testing methods are specified. For the current study, specimens of **Type B2**, were designed, as they are specified as more appropriate for multidirectional mats and fabrics. For testing, **method 2** was chosen as most appropriate for this type of specimens.

### 4.3.2 Results

Compression testing was conducted according to ISO14126 standard [3]. Coupons were placed in the Instron 1251 machine used for the testing, such as they would be loaded through in plane shear after the closure of the jaws. Caution was taken so that the major axis of the coupons was aligned to the center line of the jaws of both the loading cylinder and the traverse. The specimens were loaded at a constant displacement rate of **0.005 mm/s(0.3mm/min)**. Force-displacement data was recorded using the Mp3 software connected to the machine every 1 second while photos were taken with the same frequency. For this type of specimens, 3D DIC recording method was used, in order to be able to capture any out of plane movement that the specimens could experience during

Dimensions in millimetres

| Dimensions | Symbol | Type A specimen | Type B1 specimen | Type B2 specimen |
|---|---|---|---|---|
| Overall length (minimum) | $l_0$ | 110 ± 1 | 110 ± 1 | 125 ± 1 |
| Thickness | $h$ | 2 ± 0,2 | 2 ± 0,2 to 10 ± 0,2 | ⩾ 4 |
| Width | $b$ | 10 ± 0,5 | 10 ± 0,5 | 25 ± 0,5 |
| Distance between end tabs/grips | $L$ | 10 | 10 | 25 |
| Length of end tabs (minimum) | $l_t$ | 50 | 50 (if required) | 50 (if required) |
| Thickness of end tabs | $d_t$ | 1 | 0,5 to 2 (if required) | 0,5 to 2 (if required) |

(a) Specimen types as specified in [3].

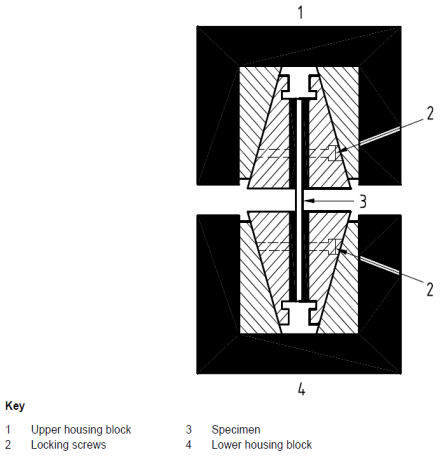


(b) Test methods as specified in [3].

Figure 19: Specimens and test design according to [3].

the loading history, due to out of plane bending or twist from the jaws pressure. Before starting the test, photos were taken succesively before and after clamping the specimens, and twist was calculated through DIC in order to realize whether it would have a large influence in the extracted results.

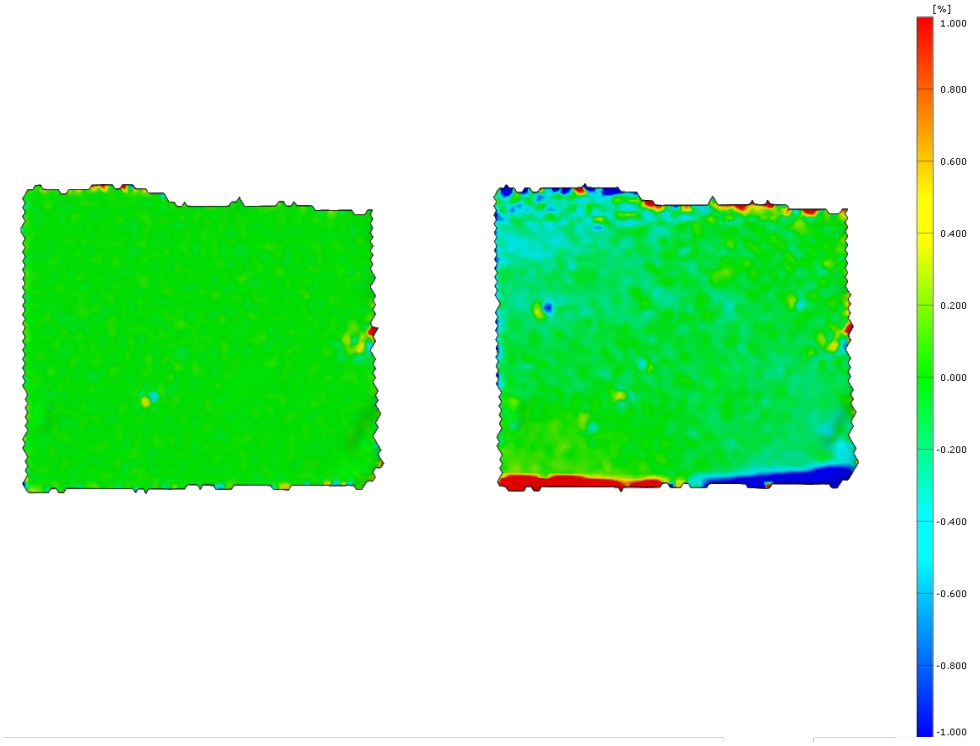


Figure 20: Out of plane strain $\epsilon_3$ before(left) and after(right) clamping.

| Coupon ID | Twist Angle(radians) |
|---|---|
| TK01 | 0.025 |
| TK02 | 0.023 |
| TK03 | 0.026 |
| TK04 | 0.024 |
| TK05 | 0.026 |
| TK06 | 0.022 |
| TK07 | 0.021 |
| TK08 | 0.011 |
| TK09 | 0.012 |
| **Mean** | **0.021** |
| **Standard Deviation** | **0.006** |
| **95% confidence interval** | **0.005** |
| **COV(%)** | **27.17** |

Table 8: Twist Angle by coupon.

The twist of the specimens after clamping, has a large influence especially in the specimen edges as can also be spotted by the DIC analysis. Twist can come as a result of misalignment of the loading grips, as well as a result of uneven trimming of the specimens and occurring eccentricities. Therefore for the bending(out of plane) strain checks needed according to [3], will be considered valid if taken from the middle of the specimen in lengthwise direction.

According to [3], the tests can be considered valid, and their results reliable for statistical analysis, only if during the loading history up to failure Euler Buckling is avoided as well as the bending due to longitudinal strains in different faces falls within the limits of the following relationship

$$\left|\frac{\epsilon_{11b} - \epsilon_{11a}}{\epsilon_{11b} + \epsilon_{11a}}\right| \leq 0.1$$

where $\epsilon_{11a}$ and $\epsilon_{11b}$ are the longitudinal strains on opposite faces of the specimen.

In the current study 3D DIC was used. Therefore the need of recording both sides of the specimens to obtain relative bending strains did not exist. As long as through 3D DIC it was possible to capture all out of plane movements of the specimen, instead of using opposite faces of the specimens to obtain longitudinal strains, those were obtained from the top and bottom end of each specimen.
As can be seen in 21 for all specimens tested throughout the loading history, in between stages **100** when the specimen is clamped, and stage **300** when total failure comes and strains go beyond acceptable limits, the relative strain ratio as defined in [3] stays below **0.1**. Therefore the tested specimens are appropriate for analysis.

Failure modes in all 9 tested specimens, fell into the acceptable limits according to [3] , [6]. In most cases compressive kink bands were formed near the top or bottom tab, that extended to through thickness shear failure, as well as delamination of the outer surface plies .Specimens **TK02**, **TK03**, **TK08** and **TK09** were excluded from the statistical analysis of the experimental data, due to premature crushing of the DIC pattern of the

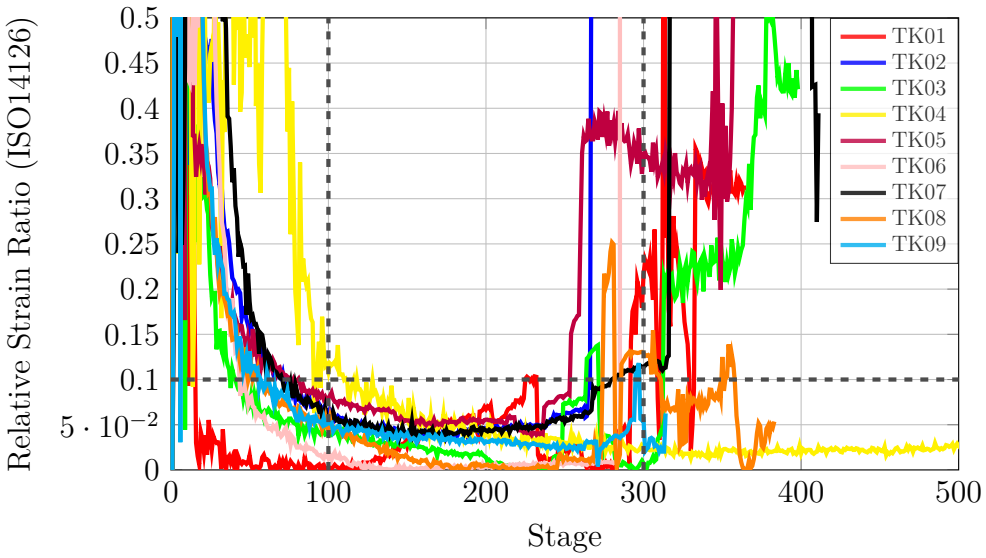


Figure 21: Relative strain ratio-recording stage.

specimens, that led to 'rigid body strains' resulting to highly nonlinear behaviour, in some cases even strain plateaus, that render the results unreliable. The available number of specimens for statistical analysis is **5**, something that agrees with the minimum requirements for sufficient testing sample according to [3].

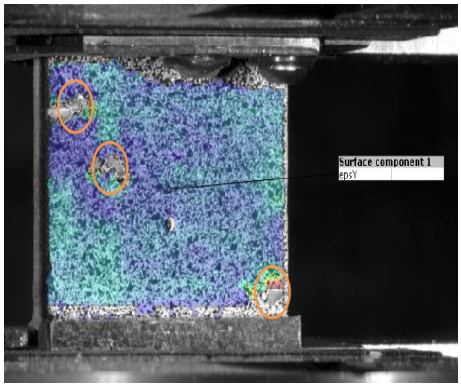


Figure 22: Crushing of the DIC pattern during testing.

According to [3] the compressive strength should be calculated as:

$$\sigma_{cM} = \frac{F_{max}}{b \cdot h}$$

Followingly the compressive modulus is defined as:

$$E_c = \frac{\sigma_c'' - \sigma_c'}{\epsilon_c'' - \epsilon_c'}$$

where $\sigma_c''$ is the compressive stress at $\epsilon_c'' = 0,0025$, and $\sigma_c'$ is the compressive stress at $\epsilon_c' = 0,0005$.

Strains were calculated along the loaded surface of the specimen, using virtual extensometers through the DIC analysis software GOM Correlate, similarly as in the case of tensile specimens.

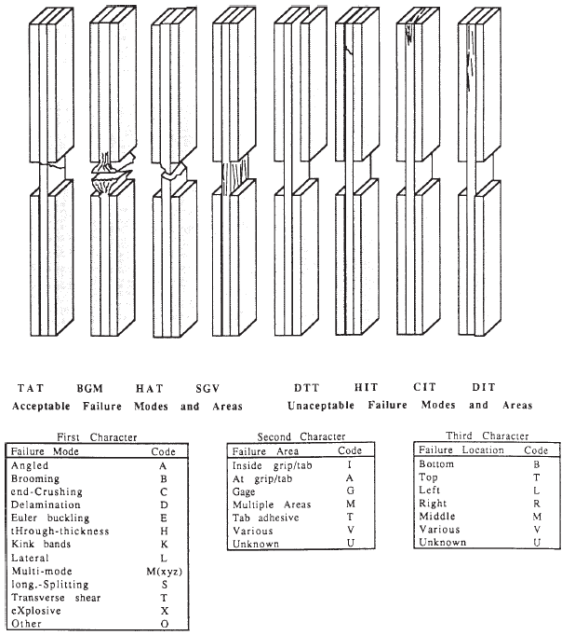

TAT BGM HAT SGV DTT HIT CIT DIT
Acceptable Failure Modes and Areas Unaceptable Failure Modes and Areas

First Character

| Failure Mode | Code |
|---|---|
| Angled | A |
| Brooming | B |
| end-Crushing | C |
| Delamination | D |
| Euler buckling | E |
| tHrough-thickness | H |
| Kink bands | K |
| Lateral | L |
| Multi-mode | M(xyz) |
| long.-Splitting | S |
| Transverse shear | T |
| eXplosive | X |
| Other | O |

Second Character

| Failure Area | Code |
|---|---|
| Inside grip/tab | I |
| At grip/tab | A |
| Gage | G |
| Multiple Areas | M |
| Tab adhesive | T |
| Various | V |
| Unknown | U |

Third Character

| Failure Location | Code |
|---|---|
| Bottom | B |
| Top | T |
| Left | L |
| Right | R |
| Middle | M |
| Various | V |
| Unknown | U |

Figure 23: Three-part failure identification codes from ASTMD3410.

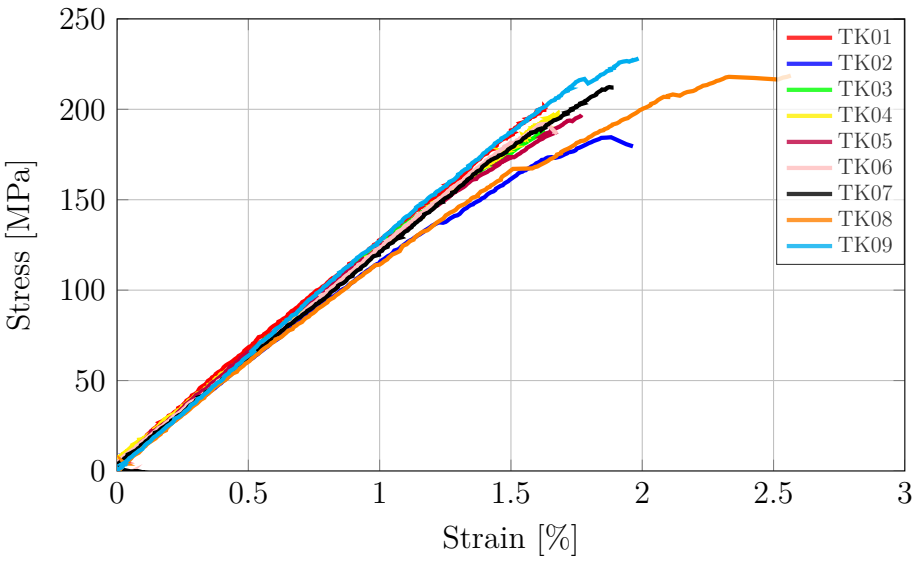


Figure 25: C Stress-Strain graph.

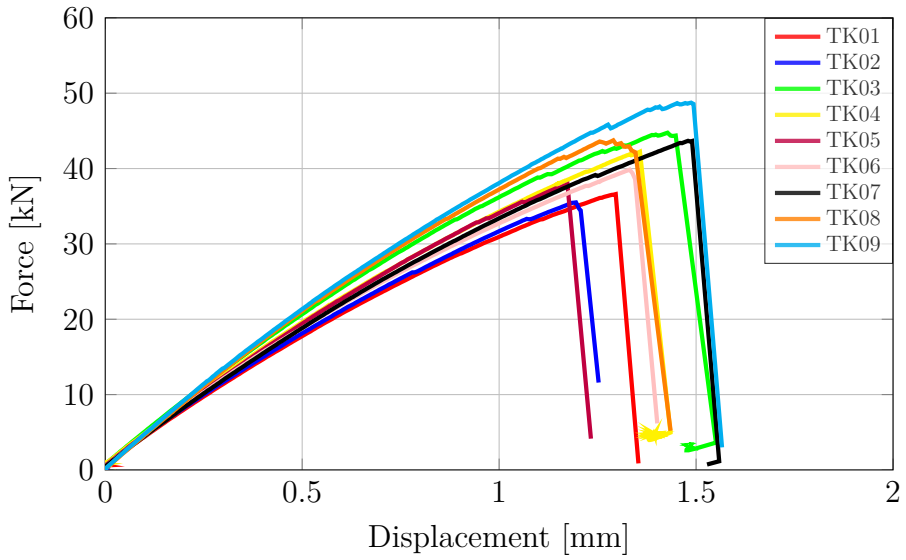


Figure 24: C Force-Displacement graph.

| **Coupon** | **Compressive Modulus (MPa)** | **Compressive strength (MPa)** | **Strain at failure(%)** | **Failure Mode** |
|---|---|---|---|---|
| TK01 | 12719.58 | 201.21 | 1.75 | HAB |
| TK02 | - | - | - | H(K)AB |
| TK03 | - | - | - | HAT |
| TK04 | 11915.85 | 198.12 | 1.63 | HAT |
| TK05 | 12554.84 | 196.97 | 1.85 | HAT |
| TK06 | 11763.65 | 191.96 | 1.63 | HAT |
| TK07 | 11431.63 | 212.29 | 1.82 | HAB |
| TK08 | - | - | - | HAM |
| TK09 | - | - | - | HAM |
| **Mean** | **12077.11** | **200.11** | **1.73** | |
| **Standard Deviation** | 543.58 | 7.58 | 0.10 | |
| **95% confidence interval** | 476.46 | 6.64 | 0.092 | |
| **COV(%)** | 4.50 | 3.78 | 6.03 | |

Table 9: Results of Compressive testing.

Results of the specimens used for the statistical analysis present good correlation. Compressive stiffness results are in good agreement with the Elastic Moduli results from the Tensile tests as expected. Compressive strength values of **200.1± 6.6 MPa** are somewhat smaller than the tensile ones implying that the fibres are most prone to compressive crushing . This was to be expected mainly due to the compressive buckling of the fibres , forming kink bands and prematurely fail. Over all the results can be considered reliable and furthermore can be used for material modelling purposes.

## 4.4 Compact Tension (CT) tests

### 4.4.1 Specimens dimensions

For the CT specimens the prefix **DCT** is used. A total of five(5) Doubly Tapered Compact tension specimens were tested under quasi static loading.

| Specimen ID | DCT01 | DCT02 | DCT03 | DCT04 | DCT05 |
|---|---|---|---|---|---|
| w(mm) | 76.08 | 76.00 | 75.52 | 75.58 | 74.98 |
| W(mm) | 89.88 | 89.56 | 89.58 | 89.75 | 89.7 |
| h(mm) | 6.98 | 6.84 | 6.84 | 6.97 | 6.84 |
| a(mm) | 20 | 20 | 20 | 20 | 20 |

Table 10: CT specimens dimensions.

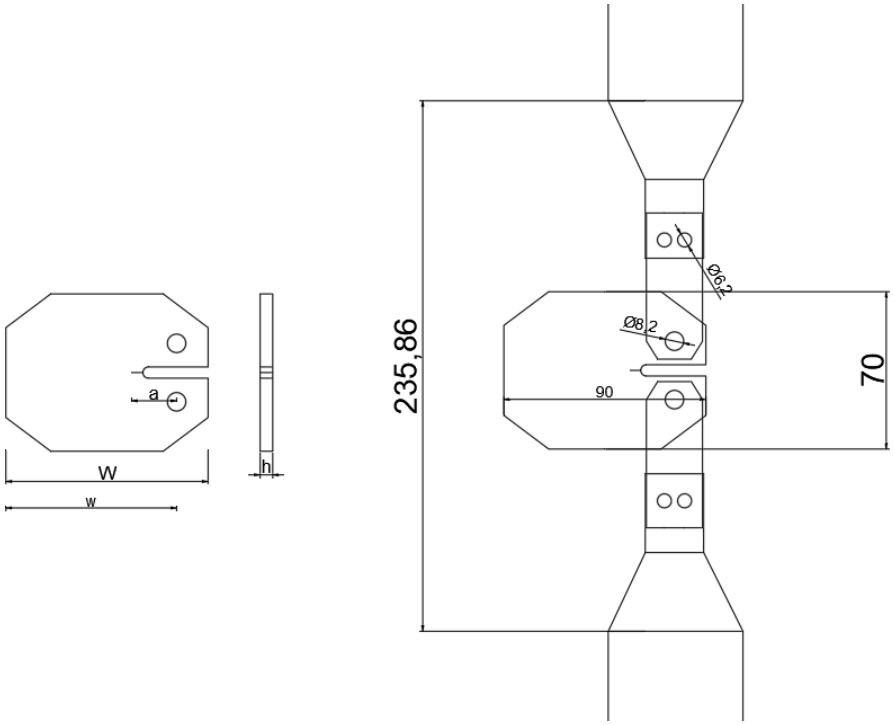


Figure 26: CT test setup.

The specimen design was based on the studies of Blanco et al. [7], [8] where the intralaminar fracture properties of woven composites, of similar structure as the ones used in the current project, were investigated. In this study, several different geometries of modified CT specimens were compared, using Finite Element Models in conjunction with the Virtual Crack Closure technique. The basis of comparison was the level up to which the different geometries would decrease unwanted failure modes such as fibre fracture due to longitudinal compressive stresses in the back of the specimen, or matrix cracking due to in plane shear stresses. Detailed specimen analysis is to be found in [7], [8] .

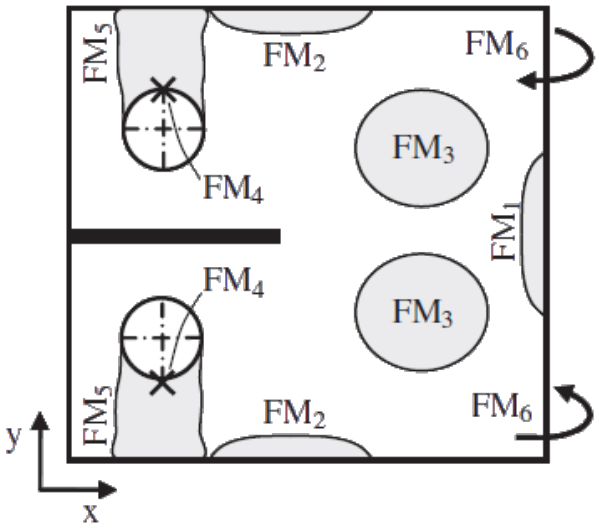


Figure 27: Failure modes to be avoided using the 2TCT specimen [7]

### 4.4.2 Results

A total of five (5) Compact Tension specimens were tested under quasi-static type of loading using the **tensile-compression press Instron 1251** located at the back of the Stevin II lab south hall. Specimens were loaded using **displacement controlled** load application, with a rate of **0.0083 mm/s** (0.50 mm/min). Force-displacement data were recorded within 1 second intervals through the Mp3 software connected to the machine, while photos using 3D Digital Image Correlation system were taken every 2 seconds. Using the 3D DIC system, any out of plane movements of the specimens, that could occur due to compression stresses at the back as well as the top and bottom edges of the specimens could be captured, and therefore not affect the in plane strain analysis producing error.

Out of the five tested specimens, 3(DCT02, DCT03, DCT04) of them presented acceptable failure modes with a crack initiating and developing along the precrack line towards the back of the specimen, while in 2(DCT01, DCT05) of the specimens, the crack once it initiated, immediately turned towards the bottom edge with final failure due to compression similar as Failure Mechanism 2 (FM2) presented in 27. Thus only the three specimens that presented acceptable failure modes were analyzed, and final intralaminar fracture toughness in mode I was calculated. This was done using three different approaches, two presented in different test standards, namely **ISO 13586** [4] and **ASTME399** [5], and the solely experimental **Compliance Calibration Method (CCM)**. The same considered force values at crack initiation were used for all three methods.

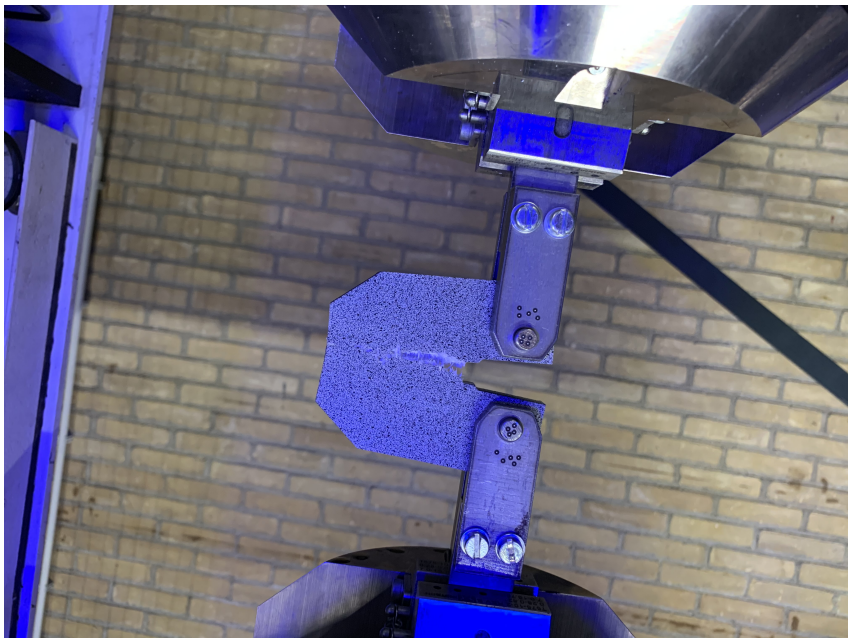

Figure 28: CT testing.

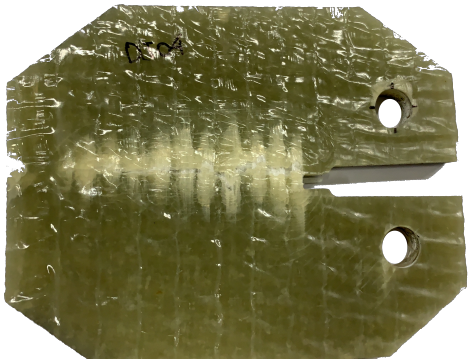

(a) Acceptable failure mode (DCT04).

(b) Unwanted failure mode (DCT01).

Figure 29: CT failure modes.

**ISO13586**

ISO 13586 [4] specifies the principles through which the Mode I translaminar fracture toughness of plastics can be determined. Although it was initially developed for non-reinforced plastics, it is considered appropriate for extracting results for fibre reinforced plastics as well. It can therefore be used for the current experimental study as well. In the standard two different testing methods are defined, namely three-point bending tests on Single End Notched specimens (**SENB**) and Compact specimens tensile tests (**CT**).

Determination of the Mode I translaminar fracture toughness $\mathbf{G}_{Ic}$ is based on calculating the area enclosed under the force-displacement curve up to the considered crack initiation load. For formation of the Force-displacement curves as presented in 30 the Crack Mouth Opening Displacement (CMOD) is extracted using the DIC analysis software GOM Correlate. Three points as shown in are drawn in both the top and the bottom of the specimens mouth and the displacement along the y axis is extracted. In this experiment only the bottom part connected to the loading cylinder moves downwards while the top

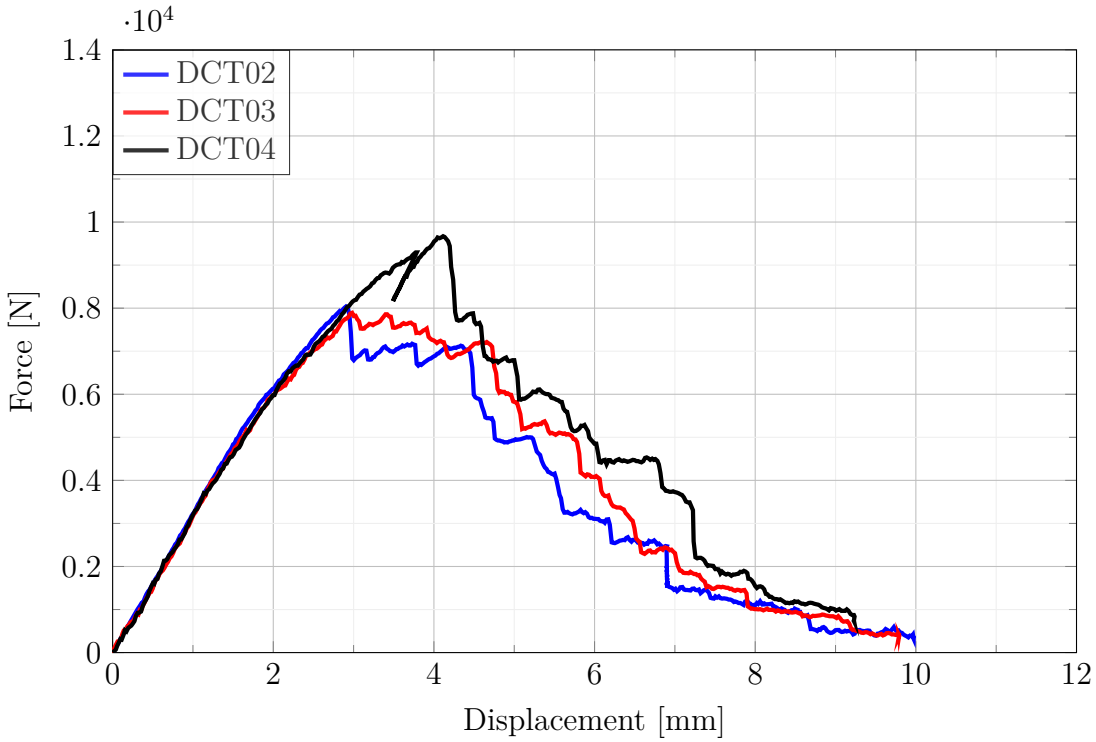


Figure 30: CT Force vs Displacement graph.

part connected to the traverse is fixed. In the top part though rotation of the specimen around the pin takes place. In order to obtain the correct CMOD therefore using the DIC analysis, the vertical displacement of the top part due to rotation, is substracted from this of the moving bottom part.

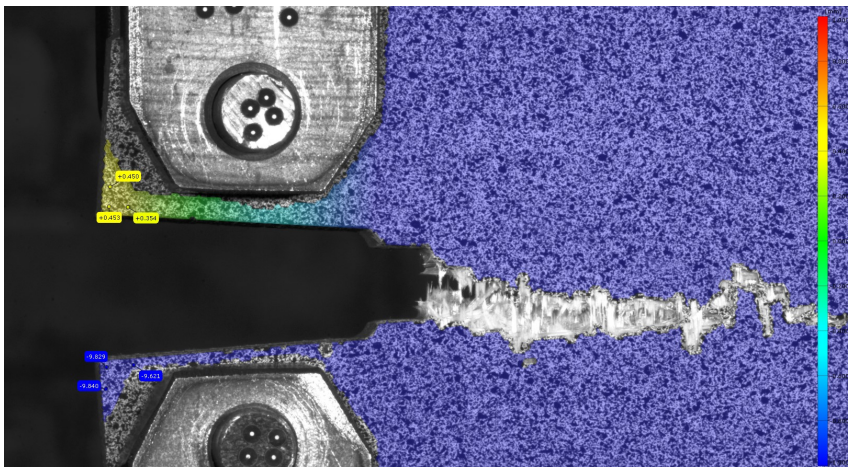

Figure 31: CMOD calculation using GOM Correlate software.

Determination of the crack initiation load takes place by comparing the maximum load attained during the loading history, with the load that corresponds to 5 % decrease in global stiffness. In the rare case where everything up to crack initiation behaves in a linear elastic manner (LEFM) the maximum load $F_{max}$ is chosen. In most case though several non-linearities can exist prior to the maximum load, and thus if the load corresponding to 5% decrease in stiffness $F_5$ falls in between the linear regime and the maximum load this is chosen instead. In any case a condition of 10% of non-linearity, $\frac{F_{max}}{F_5} < 1.1$ should

be always satisfied in order for the test to be considered valid.

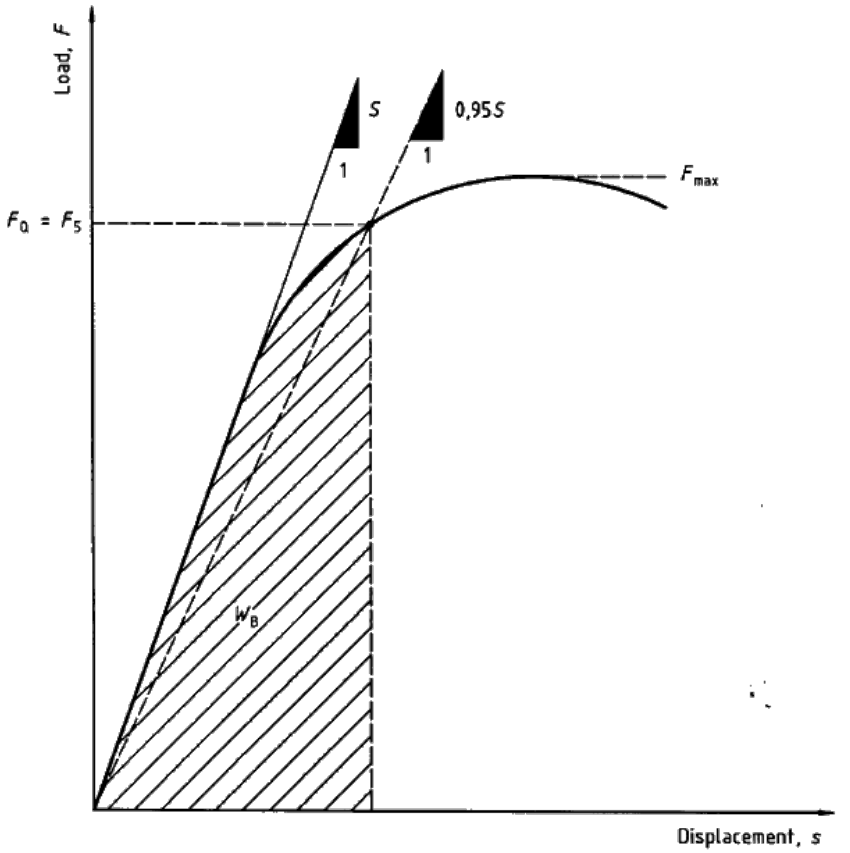


Figure 32: Typical Force-displacement curve of a notched specimen [4].

Once the initiation load has been defined and the corresponding area below the force-displacement curve $W_B$ has been calculated, the candidate Mode I translaminar fracture toughness is calculated as

$$G_Q = \frac{W_B}{h \cdot w \cdot \phi(\alpha/w)}$$

where **h,w** are the tested specimen's thickness and width respectively (depicted in 26, while $\phi$ is the energy calibration factor, dependent on the crack length $\alpha$ given in Annex A of the standard. In the given tables, fractions between 0.25 and 0.75 are given. When $\alpha/w$ falls out of the given values linear interpolation is used for determination of the $\phi$ factor.
In 11 results of $G_{Ic}$ according to ISO13586 for the three analyzed specimens are given.

$\alpha = a/w$
where
$a$ is the crack length
$w$ is the width

Interpolation is recommended.

| $\alpha$ | $f$ | $\phi$ |
|---|---|---|
| 0,25 | 4,92 | 0,199 |
| 0,30 | 5,62 | 0,208 |
| 0,35 | 6,39 | 0,213 |
| 0,40 | 7,28 | 0,213 |
| 0,45 | 8,34 | 0,208 |
| 0,50 | 9,66 | 0,199 |
| 0,55 | 11,36 | 0,186 |
| 0,60 | 13,65 | 0,170 |
| 0,65 | 16,86 | 0,152 |
| 0,70 | 21,55 | 0,133 |
| 0,75 | 28,86 | 0,112 |

Figure 33: Energy calibration factors $\phi$ for CT specimens [4].

| **ISO 13586** | | |
|---|---|---|
| **Specimen ID** | $P_{ini}$ [N] | **$G_{Ic}$ [N/mm]** |
| DCT02 | 6135 | 56.16 |
| DCT03 | 6157 | 59.11 |
| DCT04 | 6665 | 75.04 |
| **Average** | - | **63.44** |
| **St. Dev** | - | 8.29 |
| **COV(%)** | - | 13.07 |
| **95% conf. interval** | - | 9.38 |

Table 11: $G_{Ic}$ according to ISO 13586.

**ASTME399**
ASTME399 is a test standard for calculation of the Mode I linear elastic fracture toughness for metallic isotropic materials. The material system used in the current study comprises of quasi-isotropic woven laminates and therefore application of it is recommended. When it comes to fibre reinforced plastics it is used in conjuction with ASTMD5045 [9], test standard for fracture toughness calculation of plastic materials. In that case ASTME399 is used for calculation of the stress intensity factor in the opening mode $K_{Ic}$, while ASTMD4045 is used to transform the fracture toughness to strain energy release rate $G_{Ic}$ which is used as an equivalent expression of fracture toughness in the case of anisotropic materials.

For the considered load at crack initiation, similar principles as the aforementioned ISO standard are applied in this case as well. The load that corresponds to 5% decrease in stiffness is compared to the maximum load attained during the loading history and the lower value is defined as crack initiation point. Followingly the Stress Intensity Factor (SIF) is calculated according to [5]

$$K_{Ic} = \frac{P}{t \cdot \sqrt{w}} \cdot f(\alpha/w)$$

where **P** is the considered load at crack initiation, **t, w** are the thickness and the width (from the loading application points) of the specimen respectively, while **f** is dependent on the considered crack length and equal to

$$f\left(\frac{a}{w}\right) = \frac{\left(2+\frac{a}{w}\right)\left[0.886+4.64\frac{a}{w}-13.32\left(\frac{a}{w}\right)^2+14.72\left(\frac{a}{w}\right)^3-5.6\left(\frac{a}{w}\right)^4\right]}{\left(1-\frac{a}{w}\right)^{3/2}}$$

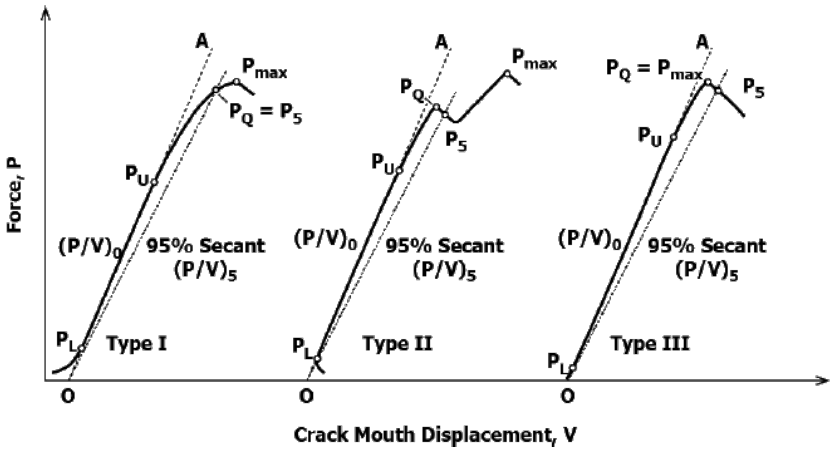


Figure 34: Crack initiation load according to ASTMD399.

Once the SIF is calculated, principles of ASTMD5045 are applied and the corresponding energy release rate is defined through its relation with the SIF, but taking into account the anisotropy of the composite laminate

$$G_{Ic}^{lam} = \frac{K_{lc}^2}{\sqrt{2E_{11}E_{22}}}\sqrt{\sqrt{\frac{E_{11}}{E_{22}}}+\frac{E_{11}}{2G_{12}}-v_{12}}$$

where $E_{11}$, $E_{22}$, $G_{12}$, $\nu_{12}$ are the elastic properties of the material defined through tensile, compression and in-plane shear testing while $K_{Ic}$ the stress intensity factor as calculated in the previous step.

| **ASTME399** | | |
|---|---|---|
| **Specimen ID** | $P_{ini}$ [N] | **$G_{Ic}$ [N/mm]** |
| DCT02 | 6135 | 27.12 |
| DCT03 | 6157 | 26.02 |
| DCT04 | 6665 | 31.24 |
| **Average** | - | **28.13** |
| **St. Dev** | - | 2.25 |
| **COV(%)** | - | 7.98 |
| **95% conf. interval** | - | 2.54 |

Table 12: $G_{Ic}$ according to ASTM E399.

**Compliance Calibration Method**

Use of the Compliance Calibration Method(CCM) for the calculation of the fracture toughness in several testing setups, has been extensively used throughout literature [10]. The big advantage of it is that is solely based on experimental data, and its not dependent on any material mechanics assumptions, making it independent of the specimens geometry

and dimensions. Downside of it is that the specimens compliance should be known for different crack lengths, making it inherently prone to crack length measurement errors. For calculation of the fracture toughness the well known Irwin-Kies equation based on LEFM is applied where P is the maximum load , C the experimentally derived compliance for different crack lengths while **B** the width of the specimen referred in the previous drawing as **w**.

$$G_I = \frac{P^2}{2B} \cdot \frac{\partial C}{\partial a}$$

The compliance used is the secant compliance calculated from the force-displacement curve, by drawing a straight line that each time connects the 0 coordinate to a point of unstable crack propagation. These points can be identified as kinks in 30. For each stage at which the compliance is measured a crack length is visually identified through the DIC analysis. Identifying the crack length in such case due to its opening nature is easier to be captured in the photos than it would be in the case of shear separation, but still can not be 100 % accurate.

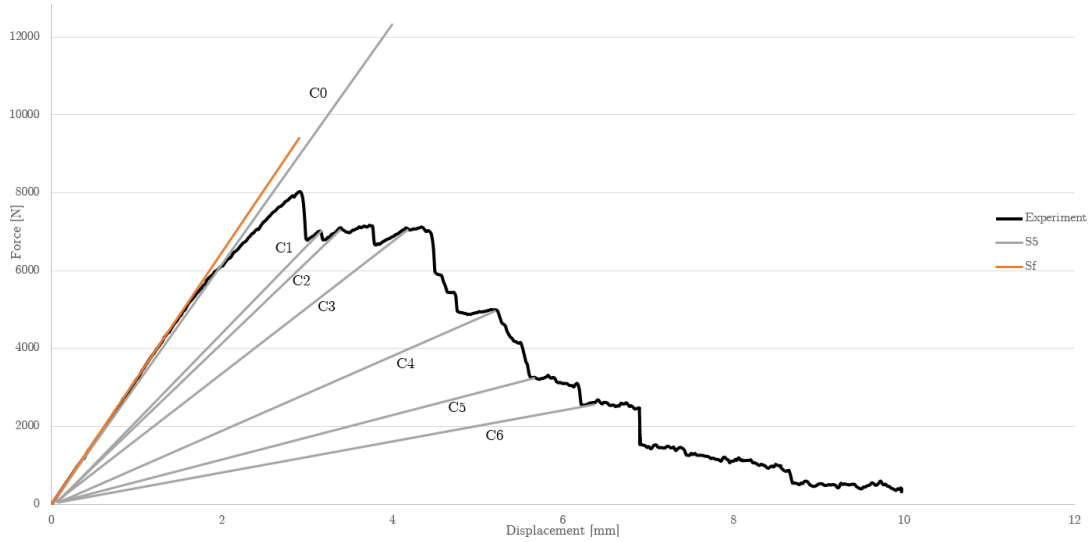


Figure 35: Compliance definition in force vs CMOD graph (DCT02).

Fitting of the compliance versus crack length data, takes place using the assumption of cubic polynomial fit $C = f(a^3)$, as also suggested by Pinho et al. in [10] and can be considered appropriate for this obtained experimental data by observing figure 36. Differentiating the Irwin-Kies equation therefore yields

$$G_{Ic} = \frac{P^2}{2 \cdot B} \cdot 3 \cdot m \cdot \alpha^2$$

where **m** corresponds to the slope factor of the cubic polynomial best fit.

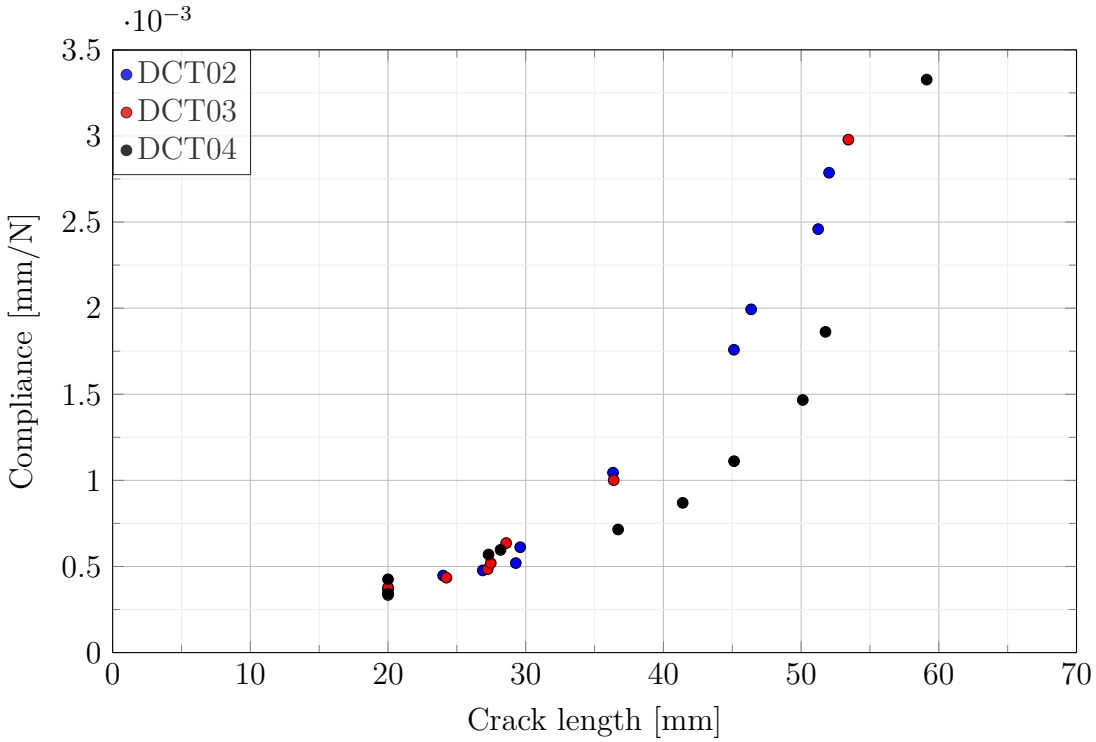


Figure 36: Compliance vs crack length.

Results of $G_{Ic}$ using the CCM are given in table 13

| **Compliance Calibration Method** | | |
|---|---|---|
| **Specimen ID** | $P_{ini}$ [N] | **$G_{Ic}$ [N/mm]** |
| DCT02 | 7019 | 70.07 |
| DCT03 | 7857 | 45.96 |
| DCT04 | 6665 | 63.74 |
| **Average** | - | **59.93** |
| **St. Dev** | - | 10.20 |
| **COV(%)** | - | 17.03 |
| **95% conf. interval** | - | 11.55 |

Table 13: $G_{Ic}$ according to CCM.

Results of all three different methods used are compared. ISO 13586 and the Compliance Calibration Method, produce quite similar results with **63.44** N/mm and **59.93** N/mm respectively. ASTMD399 produces the lower estimate of the translaminar fracture toughness with a value of **28.13** N/mm. Applicability of this method for anisotropic composite laminates can be considered questionable. This is mainly due to the fact that the fracture toughness calculation is based on the SIF formulas used for isotropic metallic materials. It can therefore be that such a simplification underestimates the results. On the other hand, ISO13586 is based in a quite straight forward consideration of the area below the force-displacement curve to represent the consumed energy for crack initiation, while the CCM is based solely on the right measurement of the specimen compliance and crack length. It has also been highlighted throughout literature [10] that use of the SIF of isotropic metals for fracture toughness calculations of fibre reinforced plastics, has many

times resulted to eroneous result not representing reality. It is therefore recommended if the ASTM standards are to be used, that the SIF around the crack tip is calculated through Finite Element Softwares such as Abaqus/CAE.

# 5 Concluding remarks

The experimental testing series presented, produced valuable results regarding the elastic and fracture properties of the FRP layup used within the Wrapped Composite Joints project. The properties extracted may be used further for realistic modelling of the material as well as interfacial behaviour of the joint in various scales. Results are in good agreement with previously established parameters through proper calibration and fitting of joint experiments through FEM. 2D and 3D DIC analysis, prove to be an effective method for accurate displacement and strain measurements in small scale scale specimens. In the case of tests like the compression and Compact tension cases, where the loading type can produce out of plane displacement, 3D DIC may be preferred over 2D DIC as shown in the presented study. In the case of tensile and compression specimens, a number of specimens failed in an unwanted way close to the grips, therefore revealing the need of more robust design of the specimens in future works, with the use of either aluminium or steel tabs to avoid such problems. Special caution should also be taken in order for the specimen tabs to be symmetric so that no misalignment occurs once the specimens are clamped. Finally in the case of Compact Tension tests, it was shown that use of different data reduction methods can produce quite different results in terms of fracture toughness values. From the findings of this work, the currently most reliable method is considered to be the one proposed in ISO standards, while use of ASTME399 should more appropriately take place in combination with numerical modelling. Compliance Calibration method, is also considered appropriate, but special care should be taken during visual crack length measurements in order for it to be accurate.

Over all the presented experimental campaign helped the author to gain more in depth knowledge on coupon testing and use of test and design standards. It was a good practice towards a final MSc thesis, where ENF tests are to be conducted, while results that were produced can well be used as input for Finite Element Models of the upcoming interface tests.

# References


[1] ISO 14129:1997(E). *Fibre-reinforced plastic composites-Determination of the in-plane shear stress/shear strain response, including the in-plane shear modulus and strength, by the ± tension test method.* Tech. rep. International Organization for Standardization, 1997.

[2] ISO 527-1:2012(E). *Plastics - Determination of tensile properties - Part 1: General principles.* Tech. rep. International Organization for Standardization, 2012.

[3] ISO 14126:1999(E). *Fibre-reinforced plastic composites —Determination of compressive properties in the in-plane direction.* Tech. rep. International Organization for Standardization, 1999.

[4] ISO 13586:2000(E). *Plastics-Determination of fracture toughness ($G_{IC}$ and $K_{IC}$)-Linear elastic fracture mechanics(LEFM) approach.* Tech. rep. International Organization for Standardization, 2000.

[5] E08 Committee. *Test Method for Linear-Elastic Plane-Strain Fracture Toughness of Metallic Materials.* ASTM International. DOI: 10.1520/E0399-20A. URL: http://www.astm.org/cgi-bin/resolver.cgi?E399-20A (visited on 04/12/2021).

[6] ASTM D3410M-03. *Standard Test Method for Compressive Properties of Polymer Matrix Composite Materials with Unsupported Gage Section by Shear Loading.* Tech. rep. American Society for Testing and Materials, 2003.

[7] N. Blanco et al. "Intralaminar fracture toughness characterisation of woven composite laminates. Part I: Design and analysis of a compact tension (CT) specimen". In: *Engineering Fracture Mechanics* 131 (Nov. 2014), pp. 349–360. ISSN: 00137944. DOI: 10.1016/j.engfracmech.2014.08.012. URL: https://linkinghub.elsevier.com/retrieve/pii/S0013794414002744 (visited on 04/11/2021).

[8] N. Blanco et al. "Intralaminar fracture toughness characterisation of woven composite laminates. Part II: Experimental characterisation". In: *Engineering Fracture Mechanics* 131 (Nov. 2014), pp. 361–370. ISSN: 00137944. DOI: 10.1016/j.engfracmech.2014.08.011. URL: https://linkinghub.elsevier.com/retrieve/pii/S0013794414002732 (visited on 04/11/2021).

[9] D20 Committee. *Test Methods for Plane-Strain Fracture Toughness and Strain Energy Release Rate of Plastic Materials.* ASTM International. DOI: 10.1520/D5045-14. URL: http://www.astm.org/cgi-bin/resolver.cgi?D5045-14 (visited on 04/12/2021).

[10] S.T. Pinho, P. Robinson, and L. Iannucci. "Fracture toughness of the tensile and compressive fibre failure modes in laminated composites". In: *Composites Science and Technology* 66.13 (Oct. 2006), pp. 2069–2079. ISSN: 02663538. DOI: 10.1016/j.compscitech.2005.12.023. URL: https://linkinghub.elsevier.com/retrieve/pii/S026635380600011X (visited on 04/11/2021).